SUPPORTING INFORMATION

April. 27, 2022

Reaction of SO_3 with $HONO_2$ and Implications for Sulfur Partitioning in the Atmosphere

Bo Long,[1] Yu Xia,[1] Junwei Lucas Bao,[2] Javier Carmona-García,[3,4] Juan Carlos Gómez Martín,[5] John, M. C. Plane,[6] Alfonso Saiz-Lopez,[4] Daniel Roca-Sanjuán,[3] Joseph S. Francisco,[7,*]

[1]College of Materials Science and Engineering, Guizhou Minzu University, 550025 Guiyang, China
[2]Department of Chemistry, Boston College, Chestnut Hill, Massachusetts 02467, United States
[3]Institut de Ciència Molecular, Universitat de València, València 46071, Spain
[4]Department of Atmospheric Chemistry and Climate, Institute of Physical Chemistry Rocasolano, CSIC, Madrid 28006, Spain
[5]Instituto de Astrofísica de Andalucía, CSIC, Granada 18008, Spain
[6]School of Chemistry, University of Leeds, LS2 9JT, Leeds, UK
[7]Department of Earth and Environmental Sciences and Department of Chemistry, University of Pennsylvania, Philadelphia, Pennsylvania 19104, United States

TABLE OF CONTENTS

Computational Methods

Electronic structure calculations. Benchmark calculations were carried out with the W2X[1]//DF-CCSD(T)-F12b[2,3]/jun′-cc-pVDZ method. Geometry optimizations and frequency calculations were performed at DF-CCSD(T)-F12b/jun′-cc-pVDZ level pf theory and single point energy calculations were done by using the W2X composite method very close to the CCSD(T, FULL)/CBS accuracy. DF-CCSD(T)-F12b/jun′-cc-pVDZ has been chosen for geometrical optimization and frequency calculations because our previous investigations have shown that DF-CCSD(T)-F12b/jun′-cc-pVDZ, where jun′-cc-pVDZ basis set is a revision of jun-cc-pVDZ. Here, the original DF-CCSD(T)-F12b/jun-cc-pVDZ calculations are done by using "cc-pVDZ/JKfit", "cc-VDZ/MP2fit", and "cc-pVDZ/OptR1" as auxiliary basis sets. DF-CCSD(T)-F12b/jun′-cc-pVDZ is defined by using "aug-cc-pVDZ/JKfit", "aug-cc-pVDZ/MP2fit", and "aug-cc-pVDZ/OptR1" as auxiliary basis sets. In our previous investigation, DF-CCSD(T)-F12b/jun-cc-pVDZ can reach the accuracy of CCSD(T)-F12a/cc-pVTZ-F12.[4]

Rate theory calculations. Canonical variational transition state theory with small-curvature tunneling was used to account for re-crossing effects and tunneling at the validated M08-HX/MG3S[5,6] functional method. High-pressure-limit rate constants were calculated by using the dual-level strategy developed by our group[7,8] that combines transition state theory without tunneling at the W2X//DF-CCSD(T)-F12b/jun′-cc-pVDZ level with variational transition state theory with small-curvature tunneling at the M08-HX/MG3S level. The pressure-dependent rate constants were calculated by using system-specific quantum Rice-Ramsperger-Kassel (SS-QRRK) theory.[9,10,11] F_E is the thermal fraction of unimolecular states above the threshold energy and is defined in Troe' s,[12] which is computed based on numerically integrated Whitten-Rabinovitch approximation.[13]

The collision efficiency was computed based on the Gilbert-Luther-Troe model,[14] with the energy transfer parameter $<\triangle E>_{down}$ = 200 cm^{-1}. The Lennard-Jones (L-J) parameters for N_2 (bath gas) were taken as ε = 82 K, σ = 3.74 Å,[15] and for the adduct as ε = 292 K, σ = 3.7 Å. The L-J parameters for the adduct were estimated from ε (SO_3) = 218.1 K, σ (SO_3) = 3.13 Å,[16] ε (HNO_3) = 390 K, and σ (HNO_3) = 4.24 Å[17] using the empirical Lorentz-Berthelot combination rules[18]. Scale factors of 0.981 and 0.973 were used to correct the calculated zero-point vibrational energies for DF-CCSD(T)-F12b/jun′-cc-pVDZ and M08-HX/MG3S, respectively.[19] In addition, the pressure dependence was evaluated by the energy-grained master equation (ME) with the direct diagonalization method (diagonalization of the global relaxation matrix to obtain chemically significant eigenmodes[20]). In the calculations, microcanonical rate constants are used, which were computed by Rice-Ramsperger-Kassel-Marcus (RRKM) theory[21] with parameters from W2X//DF-CCSD(T)-F12b/jun′-cc-pVDZ. The falloff effects agree well with each other in both methods as shown in Table A1. [22]

All the electronic structure calculations were performed by using the *Gaussian* 16[23] for M08-HX/MG3S and using the *Molpro* 2019[24] for W2X. The rate constant calculations were executed by using the *Polyrate* 2017-C[25] and *Gaussrate* 2017-B,[26] while The RRKM and master equation was computed by using the *MESS*.[27]

Computation of cross-sections and photodissociation rates. The ultraviolet and visible (UV/Vis) electronic absorption spectrum and cross-sections (σ/cm^2) of the P1 product were determined by means of a nuclear ensemble approach[28,29] previously benchmarked[30] and applied to several systems of atmospheric interest[31,32,33,34] including the $HOSO_2$ radical.[35] This computational strategy is based on the nuclear sampling of the optimized ground-state equilibrium structure according to a Wigner distribution[36] using the corresponding vibrational harmonic frequencies of the normal modes. Once a representative ensemble of structures is obtained, vertical excitation energies (ΔE) and oscillator strengths (f) of the considered electronic excited states are computed at each sampled geometry. Then, the corresponding absorption cross-section at each photon energy E ($\sigma(E)$) is calculated using the following equation:[37]

$$\sigma(E) = \frac{1}{N_p}\sum_{k}^{N_p}\frac{\pi e^2}{2mc\varepsilon_0}\sum_{l\neq 0}^{N_{fs}} f_{0l}(R_k)\, g(E-\Delta E_{0l}(R_k),\delta) \qquad (1)$$

where N_p is the number of sampled geometries, m and e the mass and charge of the electron, c the speed of light in vacuum, ε_0 the vacuum permittivity, N_{fs} the number of excited states, $f_{0l}(R_k)$ the oscillator strength of the transition from the ground state to the

l-th excited state for each geometry R_k and $g(E-\Delta E_{0l}(R_k),\delta)$ is a Gaussian type shape function which accounts for the broadening of the resonant lines of the spectra represented by δ. This Gaussian function depends on the nature of the transition and is centered at the vertical transition energy to a particular l-th excited state $\Delta E_{0l}(R_k)$.

The optimized ground-state equilibrium geometry and corresponding vibrational frequencies were computed at the B3LYP[38,39]/6-311+G(3df)[40,41,42] level of theory with the Gaussian 16 (revision A0.3) software package.[23] The Newton X 2.0 program[43,44] was used to carry out the Wigner nuclear sampling at 0 K, obtaining a set of 200 representative geometries. The broadening of the Gaussian shape function, δ, was set to a value of 0.15 eV. This value was chosen for being the smallest one that does not produce any unphysical peaks.

Regarding the level of theory used to compute ΔE and f, the state-average complete-active-space self-consistent field/multi-state complete-active space second-order perturbation theory (SA-CASSCF[45,46]/MS-CASPT2[47,48,49,50,51]) method was employed in combination with the the atomic natural orbital-large basis set of valence double zeta with polarization functions (ANO-L-VTZP)[52,53] using the OpenMolcas software package in its 18.09 version.[54,55] In the SA-CASSCF calculations, an active space of 16 electrons in 11 orbitals i.e. CAS(16,11) was chosen and 12 roots (spin-free singlet states) were averaged without symmetry restrictions (C1 group). Note that spin-free refers in the context of the present work to the wavefunctions with a pure spin multiplicity (singlet, doublet, triplet, quartet…). For the MS-CASPT2 calculations, an ionization potential electron affinity (IPEA) shift of 0.25 a.u, was set to correct the errors in energy differences between closed and open-shell systems[56], and an imaginary level shift of 0.2 a.u. was applied to minimize the effect of weakly-interacting intruder states[57].

With the computed σ, the photolysis rate (J/s^{-1}) of the P1 product was estimated according to the following expression:[58]

$$J = \int \emptyset(\lambda,T)\sigma(\lambda,T)F(\theta,\lambda)d\lambda \quad (2)$$

where $\emptyset$ is the quantum yield for the photolysis of the species and σ is the calculated absorption cross-section. Both parameters are a function of the wavelength (λ) and temperature (T). F denotes the solar actinic flux as a function of the solar zenith angle (θ) and wavelength (λ). The value of J was computed with an in-house program over the altitude range in which the SO_3 + $HONO_2$ reaction can compete with the SO_3 + nH_2O reaction (20-40 km). A value of $\emptyset = 1$ was considered as an approximation. The solar

actinic flux spectrum at each altitude was obtained with the online version of the TUV photolysis code considering a solar zenith angle of 0º.[59]

Fitting of high-pressure-limit rate constant and calculated activation energies

The high-pressure-limit rate constants in the temperature range from 190 K to 350 K were fitted to the equation:[60,61,62]

$$k = 2.21 \times 10^{-16}\left(\frac{T + 41.03}{300}\right)^{1.879} \exp\left[-\frac{-3.487\,(T + 41.03)}{R(T^2 + 41.03^2)}\right] \quad (3)$$

where R is the gas constant (1.9872×10^{-3} kcal mol^{-1} K^{-1}) and T is temperature in K. The corresponding Arrhenius activation energies were calculated by using the expression:

$$E_a = -R\,\frac{\mathrm{d}\ln k}{\mathrm{d}\,(1/\mathrm{T})} \quad (4)$$

Fitting the pressure-dependent rate constant k(T, p) to analytical functions

The pressure-dependent rate constant $k(T, p)$ was calculated by using the following interpolating equation:

$$k(T, p) = \frac{p^2 + B(T)d(T)p}{p^2 + d(T)}\; k_\infty(T) \quad (5)$$

in which

$$B(T) = \frac{k_0(\mathrm{T})}{k_\infty(\mathrm{T})RT} \quad (6)$$

and

$$d(T) = \frac{[p_{1/2}(T)]^2}{1 - 2Bp_{1/2}(T)} \quad (7)$$

where the $k_\infty(T)$, $k_0(T)$, and $p_{1/2}(T)$ are the high-pressure-limit rate constant, the low-pressure-limit rate constant and transition pressure, respectively; R is the ideal gas constant (1.38×10^{-22} bar cm^3 molecule^{-1} K^{-1}, this may also be called the Boltzmann constant), p is in bar, B is in units of bar^{-1}, and d is in bar^2. The functional forms of $k(T, p)$ are as in our previous study.[63]

Atmospheric concentrations of P1 under different SO3 scenarios

The steady-state concentration of P1 was calculated using the calculated equilibrium constant as follows:

$$K_{eq4} = \frac{[P1]}{[\mathrm{SO_3}][\mathrm{HONO_2}]} \quad (8)$$

where K_{eq4} is the equilibrium constant in Table A2 and [SO_3], [$HONO_2$], and [P1] are the concentrations of sulfur trioxide, nitric acid, and P1, respectively. Although the concentration of sulfur trioxide remains unknown at different altitudes, experimental observations have shown that the concentration of sulfur trioxide can reach 10^6 molecules cm^{-3} in the troposphere.[64] Moreover, water vapor concentrations significantly decrease with increasing of altitude. Therefore, the concentration of sulfur trioxide should be higher in the stratosphere than in the troposphere. SO_3 concentrations would increase as a result of geoengineered injection of SO_2 or SO_3. Therefore, we have calculated the concentrations of P1 according to concentrations of sulfur trioxide in the concentration range from 10^7 to 10^{14} molecules cm^{-3} as shown in Figure S4.

Table A1. Calculated $k(T, p)$ (unit: cm^3 $molecule^{-1}$ s^{-1}) as functions of altitude from different theoretical methods.

H[a] (km)	T[a] (K)	p^a (mbar)	$k_1(T, p)^b$	$k_2(T, p)^c$	$k_{\infty1}(T)^d$	$k_{\infty2}(T)^e$	$k_{\infty1}(T)/k_1(T, p)$	$k_{\infty2}(T)/k_2(T, p)$
0	290.2	1013	1.89E-13	2.95E-13	2.31E-13	4.53E-13	1.22	1.54
5	250.5	495.9	5.05E-13	1.00E-12	5.87E-13	1.36E-12	1.16	1.36
10	215.6	242.8	1.68E-12	4.54E-12	1.89E-12	5.59E-12	1.12	1.23
15	198	118.8	3.59E-12	1.19E-11	4.11E-12	1.46E-11	1.14	1.22
20	208	58.18	1.92E-12	5.55E-12	2.59E-12	8.24E-12	1.35	1.49
25	216.1	28.48	1.05E-12	2.80E-12	1.85E-12	5.45E-12	1.77	1.95
30	221.5	13.94	5.82E-13	1.59E-12	1.50E-12	4.23E-12	2.59	2.66
35	228.1	6.826	2.65E-13	7.94E-13	1.18E-12	3.16E-12	4.46	3.99
40	240.5	3.341	8.17E-14	2.65E-13	7.87E-13	1.94E-12	9.64	7.29
45	251.9	1.636	2.50E-14	9.10E-14	5.64E-13	1.30E-12	22.53	14.29
50	253.7	0.801	1.17E-14	5.34E-14	5.37E-13	1.23E-12	45.90	22.97

[a]Data is from Brasseur, G. P.; Solomon, S., *Aeronomy of the middle atmosphere: Chemistry and physics of the stratosphere and mesosphere*. Springer Science & Business Media: 2006; pp. 617-621.

[b]The $k_1(T, p)$ is calculated by the dual-level CVT/SCT/SS-QRRK method.

[c]The $k_2(T, p)$ is calculated by the ME/RRKM method.

[d]The $k_{\infty1}(T)$ is high-pressure-limit rate constant (unit: cm^3 $molecule^{-1}$ s^{-1}) obtained by dual-level strategy.

[e]The $k_{\infty2}(T)$ is calculated by the ME/RRKM method.

Table A2. Equilibrium constant of P1 with respect to SO_3 and $HONO_2$ at different altitudes.

H[a] (km)	T[a] (K)	p^a (mbar)	K_{eq4}[b] (molecules cm^{-3})	$[HONO_2]$[a] (molecules cm^{-3})
0	290.2	1013	4.21E-19	3.80E+08
5	250.5	495.9	1.17E-17	1.50E+08
10	215.6	242.8	6.27E-16	1.90E+09
15	198	118.8	8.09E-15	1.30E+09
20	208	58.18	1.79E-15	5.50E+09
25	216.1	28.48	5.86E-16	4.60E+09
30	221.5	13.94	2.92E-16	2.30E+09
35	228.1	6.826	1.30E-16	5.80E+08
40	240.5	3.341	3.23E-17	5.70E+07
45	251.9	1.636	1.02E-17	2.50E+06
50	253.7	0.801	8.57E-18	1.60E+05

[a] Data is from Brasseur, G. P.; Solomon, S., *Aeronomy of the middle atmosphere: Chemistry and physics of the stratosphere and mesosphere*. Springer Science & Business Media: 2006; pp. 617-621

[b]The equilibrium constant calculated by the dual-level CVT/SCT/SS-QRRK method.

Table S1. Activation enthalpy at 0 K ($\Delta H_0^{\ddagger}$) and barrier height ($\Delta V^{\ddagger}$) for the SO_3 + $HONO_2$ reaction. (unit: kcal/mol)

Method	TS1	
	$\Delta H_0^{\ddagger}$	$\Delta V^{\ddagger}$
W2X//DF-CCSD(T)-F12b/jun′-cc-pVDZ	-3.19	-2.56
M08-HX/MG3S	-3.90	-2.79

Table S2. Tunneling transmission coefficients and rate constants (s^{-1}) for TS1 at various temperatures

T/K	$k_{\mathrm{TST}}^{\mathrm{HL}}$[a]	Γ_{CVT}^{LL}[b]	$\kappa_{\mathrm{SCT}}^{\mathrm{LL}}$[c]	k_1[d]	κ_{c1}	k_{-1}[e]
190	3.73E-12	3.23E-01	5.13E+00	6.18E-12	3.05E-14	2.02E+02
200	2.44E-12	3.44E-01	4.43E+00	3.73E-12	5.92E-15	6.29E+02
210	1.67E-12	3.64E-01	3.90E+00	2.38E-12	1.35E-15	1.76E+03
220	1.19E-12	3.83E-01	3.49E+00	1.59E-12	3.53E-16	4.50E+03
230	8.73E-13	4.00E-01	3.17E+00	1.11E-12	1.04E-16	1.06E+04
240	6.60E-13	4.17E-01	2.90E+00	7.98E-13	3.41E-17	2.34E+04
250	5.11E-13	4.33E-01	2.69E+00	5.94E-13	1.23E-17	4.84E+04
260	4.05E-13	4.47E-01	2.51E+00	4.54E-13	4.79E-18	9.48E+04
270	3.27E-13	4.61E-01	2.36E+00	3.55E-13	2.01E-18	1.77E+05
280	2.69E-13	4.74E-01	2.23E+00	2.84E-13	9.01E-19	3.15E+05
290	2.25E-13	4.86E-01	2.12E+00	2.31E-13	4.28E-19	5.41E+05
298	1.97E-13	4.95E-01	2.04E+00	1.99E-13	2.45E-19	8.12E+05
300	1.91E-13	4.98E-01	2.02E+00	1.92E-13	2.14E-19	8.95E+05
310	1.64E-13	5.08E-01	1.94E+00	1.61E-13	1.12E-19	1.43E+06
320	1.42E-13	5.18E-01	1.87E+00	1.37E-13	6.15E-20	2.23E+06
330	1.25E-13	5.28E-01	1.80E+00	1.18E-13	3.50E-20	3.38E+06
340	1.10E-13	5.37E-01	1.74E+00	1.03E-13	2.07E-20	5.00E+06
350	9.86E-14	5.45E-01	1.69E+00	9.09E-14	1.26E-20	7.22E+06

[a] $k_{\mathrm{TST}}^{\mathrm{HL}}$ is the conventional transition state theory without a transmission coefficient at the W2X//DF-CCSD(T)-F12b/DF-CCSD(T)-F12b/jun′-cc-pVDZ level.

[b] $\Gamma_{\mathrm{CVT}}^{\mathrm{LL}}$ is the recrossing transmission coefficient, which equals $k_{\mathrm{CVT}}^{\mathrm{LL}}/k_{\mathrm{TST}}^{\mathrm{LL}}$ at the M08-HX/MG3S level.

[c] $\kappa_{\mathrm{SCT}}^{\mathrm{LL}}$ is the tunneling transmission coefficient calculated by small-curvature tunneling approximation at the M08-HX/MG3S level.

[d] The HPL rate constant $k_1 = k_{\mathrm{TST}}^{\mathrm{HL}}\,\kappa_{\mathrm{SCT}}^{\mathrm{LL}}\,\Gamma_{\mathrm{CVT}}^{\mathrm{LL}}$, and HL is W2X//DF-CCSD(T)-F12b/DF-CCSD(T)-F12b/jun′-cc-pVDZ, LL is M08-HX/MG3S level.

[e] k_{-1} denotes the reverse rate constant.

Table S3. High-pressure-limit rate constants ($k_\infty(T)$, cm^3 $molecule^{-1}$ s^{-1}) and activation energies (E_a, kcal/mol) of the SO_3 + $HONO_2$ reaction between 190 and 350 K

T/K	$k_\infty(T)$	E_a
190	6.18×10^{-12}	-3.83
200	3.73×10^{-12}	-3.77
210	2.38×10^{-12}	-3.72
220	1.59×10^{-12}	-3.67
230	1.11×10^{-12}	-3.61
240	7.98×10^{-13}	-3.56
250	5.94×10^{-13}	-3.5
260	4.54×10^{-13}	-3.45
270	3.55×10^{-13}	-3.39
280	2.84×10^{-13}	-3.34
290	2.31×10^{-13}	-3.28
298	1.99×10^{-13}	-3.24
300	1.92×10^{-13}	-3.23
310	1.61×10^{-13}	-3.18
320	1.37×10^{-13}	-3.13
330	1.18×10^{-13}	-3.07
340	1.03×10^{-13}	-3.02
350	9.09×10^{-14}	-2.97

Table S4. Pressure and temperature dependence of $k_4(T, p)$

p (Pa)	T = 350 K	T = 320 K	T = 298 K	T = 280 K
8.01E+01	2.76E-16	7.87E-16	1.79E-15	3.68E-15
1.64E+02	5.59E-16	1.58E-15	3.58E-15	7.34E-15
3.34E+02	1.12E-15	3.14E-15	7.03E-15	1.43E-14
6.83E+02	2.20E-15	6.08E-15	1.34E-14	2.67E-14
1.39E+03	4.20E-15	1.12E-14	2.41E-14	4.67E-14
2.85E+03	7.60E-15	1.95E-14	4.01E-14	7.50E-14
5.82E+03	1.29E-14	3.11E-14	6.11E-14	1.10E-13
1.19E+04	2.02E-14	4.58E-14	8.56E-14	1.47E-13
2.43E+04	2.97E-14	6.29E-14	1.12E-13	1.84E-13
4.96E+04	4.08E-14	8.07E-14	1.36E-13	2.16E-13
1.01E+05	5.25E-14	9.74E-14	1.58E-13	2.42E-13
5.00E+05	7.50E-14	1.24E-13	1.86E-13	2.72E-13
1.00E+06	8.13E-14	1.30E-13	1.92E-13	2.78E-13
5.00E+06	8.85E-14	1.36E-13	1.97E-13	2.83E-13
1.00E+07	8.96E-14	1.36E-13	1.98E-13	2.84E-13
1.00E+08	9.08E-14	1.37E-13	1.99E-13	2.84E-13
p (Pa)	T = 260 K	T = 240 K	T = 220 K	T = 200 K
8.01E+01	8.73E-15	2.27E-14	6.72E-14	2.38E-13
1.64E+02	1.73E-14	4.44E-14	1.30E-13	4.51E-13
3.34E+02	3.32E-14	8.38E-14	2.39E-13	8.02E-13
6.83E+02	6.06E-14	1.49E-13	4.08E-13	1.30E-12
1.39E+03	1.02E-13	2.41E-13	6.27E-13	1.88E-12
2.85E+03	1.57E-13	3.51E-13	8.66E-13	2.44E-12
5.82E+03	2.18E-13	4.64E-13	1.09E-12	2.90E-12
1.19E+04	2.80E-13	5.67E-13	1.26E-12	3.23E-12
2.43E+04	3.34E-13	6.50E-13	1.39E-12	3.45E-12
4.96E+04	3.78E-13	7.10E-13	1.48E-12	3.58E-12
1.01E+05	4.09E-13	7.49E-13	1.53E-12	3.65E-12
5.00E+05	4.43E-13	7.87E-13	1.58E-12	3.71E-12
1.00E+06	4.48E-13	7.92E-13	1.58E-12	3.72E-12
5.00E+06	4.53E-13	7.97E-13	1.59E-12	3.72E-12
1.00E+07	4.54E-13	7.98E-13	1.59E-12	3.72E-12
1.00E+08	4.54E-13	7.98E-13	1.59E-12	3.73E-12

[a] The $k(T, p)$ is calculated by the dual-level CVT/SCT/SS-QRRK method.

Table S5. The fitted $k_4(T, p)$ from eq. (3) (unit: cm^3 $molecule^{-1}$ s^{-1}) at different temperatures

T/K	$k_{\infty 4}(T)$	$k_0(T)$	$p_{1/2}$	B(T)	d(T)	$k_4(T, p)$
190	6.18E-12	1.77E-29	0.0103	1.09E+02	-8.47E-05	3.09E-12
200	3.73E-12	8.89E-30	0.0136	8.64E+01	-1.37E-04	1.86E-12
210	2.38E-12	4.78E-30	0.0176	6.95E+01	-2.14E-04	1.19E-12
220	1.59E-12	2.69E-30	0.023	5.59E+01	-3.37E-04	7.94E-13
230	1.11E-12	1.60E-30	0.0296	4.55E+01	-5.18E-04	5.53E-13
240	7.98E-13	9.77E-31	0.0384	3.70E+01	-8.02E-04	3.99E-13
250	5.94E-13	6.21E-31	0.0497	3.03E+01	-1.23E-03	2.97E-13
260	4.54E-13	4.04E-31	0.0643	2.48E+01	-1.89E-03	2.27E-13
270	3.55E-13	2.70E-31	0.0827	2.04E+01	-2.88E-03	1.78E-13
280	2.84E-13	1.82E-31	0.1082	1.66E+01	-4.53E-03	1.42E-13
290	2.31E-13	1.26E-31	0.1401	1.36E+01	-7.02E-03	1.16E-13
298	1.99E-13	9.34E-32	0.1737	1.14E+01	-1.02E-02	9.94E-14
300	1.92E-13	8.71E-32	0.1832	1.10E+01	-1.11E-02	9.58E-14
310	1.61E-13	6.16E-32	0.2369	8.93E+00	-1.74E-02	8.06E-14
320	1.37E-13	4.40E-32	0.3056	7.26E+00	-2.72E-02	6.87E-14
330	1.18E-13	3.16E-32	0.3963	5.86E+00	-4.31E-02	5.92E-14
340	1.03E-13	2.30E-32	0.5118	4.75E+00	-6.78E-02	5.16E-14
350	9.09E-14	1.68E-32	0.6596	3.83E+00	-1.07E-01	4.54E-14

[a]The $k_{\infty 4}(T)$ is high-pressure-limit rate constant (unit: cm^3 $molecule^{-1}$ s^{-1}), the $k_0(T)$ is low-pressure limit rate constant (unit: cm^6 $molecule^{-1}$ s^{-1}) and $p_{1/2}$ (unit: bar).

Table S6. The fitting four-parameters of $k(T, p)$

	$SO_3 + HONO_2$ reaction			
	ln A	n	T_0	E
$k_{\infty 4}(T)$	-36.05	1.879	41.03	-3.487
$k_0(T)$	-74.56	-7.31	24.16	-1.991
$p_{1/2}$	11.74	5.033	458.5	10.57

[a] ln A (with A in s^{-1}), n (unitless), E (kcal/mol), and T_0 (K) are the four fitting parameters.

Table S7. Rate constants (units: cm^3 $molecule^{-1}$ s^{-1}) of the SO_3 + $HONO_2$ reaction, $HONO_2$ concentrations (unit: molecules cm^{-3}), and atmospheric lifetimes of SO_3 (τ_1, s) in an environment of atmospheric $HONO_2$ as functions of altitude.

SO_3+HNO_3						Lat = 60	Lon = 150		
Altitude	T	p							
(km)	(K)	(mbar)	k_4(T,p)	$k_{\infty 4}(T)$	[HNO_3]	k(T,p)	$k_{\infty}(T)$	Lifetime (hrs)	Lifetime (hrs)
0	290.2	1013	1.89×10^{-13}	2.31×10^{-13}	2.94×10^{9}	5.56×10^{-4}	6.77×10^{-4}	5.00×10^{-1}	4.10×10^{-1}
5	250.5	495.9	5.05×10^{-13}	5.87×10^{-13}	1.37×10^{9}	6.93×10^{-4}	8.04×10^{-4}	4.01×10^{-1}	3.46×10^{-1}
10	215.6	242.8	1.68×10^{-12}	1.89×10^{-12}	9.87×10^{9}	1.66×10^{-2}	1.86×10^{-2}	1.68×10^{-2}	1.49×10^{-2}
15	198	118.8	3.59×10^{-12}	4.11×10^{-12}	8.47×10^{9}	3.04×10^{-2}	3.48×10^{-2}	9.13×10^{-3}	7.99×10^{-3}
20	208	58.18	1.92×10^{-12}	2.59×10^{-12}	9.14×10^{9}	1.75×10^{-2}	2.37×10^{-2}	1.59×10^{-2}	1.17×10^{-2}
25	216.1	28.48	1.05×10^{-12}	1.85×10^{-12}	5.57×10^{9}	5.83×10^{-3}	1.03×10^{-2}	4.76×10^{-2}	2.69×10^{-2}
30	221.5	13.94	5.82×10^{-13}	1.50×10^{-12}	1.83×10^{9}	1.06×10^{-3}	2.75×10^{-3}	2.61×10^{-1}	1.01×10^{-1}
35	228.1	6.826	2.65×10^{-13}	1.18×10^{-12}	2.39×10^{8}	6.33×10^{-5}	2.83×10^{-4}	4.39×10^{0}	9.83×10^{-1}
40	240.5	3.341	8.17×10^{-14}	7.87×10^{-12}	3.13×10^{7}	2.56×10^{-6}	2.47×10^{-5}	1.09×10^{2}	1.13×10^{1}
45	251.9	1.636	2.50×10^{-14}	5.64×10^{-12}	5.75×10^{5}	1.44×10^{-8}	3.24×10^{-7}	1.93×10^{4}	8.57×10^{2}
50	253.7	0.801	1.17×10^{-14}	5.37×10^{-12}	6.02×10^{4}	7.04×10^{-10}	3.23×10^{-8}	3.94×10^{5}	8.59×10^{3}
	k1 is the forward dependent-dependent rate constant for the SO_3 + HNO_3 reaction at different altitudes between 0 and 50 km.								
	k1_HPL is the forward high-limit rate constant of SO_3 + HNO_3.								

[a] Data is from Brasseur, G. P.; Solomon, S., *Aeronomy of the middle atmosphere: Chemistry and physics of the stratosphere and mesosphere*. Springer Science & Business Media: 2006; pp. 617-621.

Table S8. Rate constants of SO_3 + $HONO_2$ and OH + $HONO_2$ as functions of altitude.

H[a] (km)	T[a] (K)	p^a (mbar)	$k_4(T,p)^b$	$k_{OH}(T)^c$
0	290.2	1013	1.89×10^{-13}	1.68E-13
5	250.5	495.9	5.05×10^{-13}	3.09E-13
10	215.6	242.8	1.68×10^{-12}	7.26E-13
15	198	118.8	3.59×10^{-12}	1.09E-12
20	208	58.18	1.92×10^{-12}	5.86E-13
25	216.1	28.48	1.05×10^{-12}	3.68E-13
30	221.5	13.94	5.82×10^{-13}	2.70E-13
35	228.1	6.826	2.65×10^{-13}	2.15E-13
40	240.5	3.341	8.17×10^{-14}	1.75E-13
45	251.9	1.636	2.50×10^{-14}	1.54E-13
50	253.7	0.801	1.17×10^{-14}	1.50E-13

[a]Data is from Brasseur, G. P.; Solomon, S., *Aeronomy of the middle atmosphere: Chemistry and physics of the stratosphere and mesosphere*. Springer Science & Business Media: 2006; pp. 617-621.

[b]Rate constant of the SO_3 + $HONO_2$ reaction (R4) at different temperature and pressure. (in cm^3 $molecule_{-1}$ s^{-1})

[c]The k_{OH} is from experiment preferred values of ref 65. (in cm^3 $molecule^{-1}$ s^{-1})

[d]The concentration of sulfur trioxide. (in molecules cm^{-3})

[c]The $\tau_{OH} = 1/k_{OH}[OH]$ that is the atmosphere lifetime of the OH + HNO_3 reaction.

Table S9. Calculated $k_{-4}(T, p)$ (unit: s^{-1}) and atmosphere lifetimes (s) as functions of altitude.

H[a] (km)	T[a] (K)	p[a] (mbar)	$k_{-4}(T, p)$[b] (s^{-1})	τ_{-4}[c] (s)
0	290.2	1013	4.50E+05	2.22E-06
5	250.5	495.9	4.33E+04	2.31E-05
10	215.6	242.8	2.68E+03	3.73E-04
15	198	118.8	4.44E+02	2.25E-03
20	208	58.18	1.07E+03	9.34E-04
25	216.1	28.48	1.79E+03	5.60E-04
30	221.5	13.94	1.99E+03	5.01E-04
35	228.1	6.826	2.04E+03	4.90E-04
40	240.5	3.341	2.53E+03	3.96E-04
45	251.9	1.636	2.46E+03	4.07E-04
50	253.7	0.801	1.36E+03	7.33E-04

[a]Data is from Brasseur, G. P.; Solomon, S., *Aeronomy of the middle atmosphere: Chemistry and physics of the stratosphere and mesosphere*. Springer Science & Business Media: 2006; pp. 617-621.

[b]The $k_{-4}(T, p)$ is calculated by the dual-level CVT/SCT/SS-QRRK method.

[c]The $\tau_{-4} = 1/k_{-4}(T, p)$ that is the atmosphere lifetime of the $SO_3 + HNO_3$ reverse reaction.

Cartesian coordinates (Å) of geometric structures optimized by DF-CCSD(T)-F12b/jun′-cc-pVDZ method

HONO2

N	0.1455893628	-0.0378879745	-0.0001620727
O	0.1360534638	-1.2502170376	-0.0000536829
O	1.0657044866	0.7286180956	0.0001846446
O	-1.1112964265	0.5811596301	-0.0002628423
H	-1.7221228866	-0.1780857136	-0.0006980468

SO3

S	-0.0000002538	-0.0000088459	0.0000000000
O	-0.1619494169	-1.4259149656	0.0000000000
O	1.3158456165	0.5726918608	0.0000000000
O	-1.1538959458	0.8531969507	0.0000000000

C1

S	1.5378044307	0.0328183638	0.0000021996
O	1.8541756338	-0.5905730179	1.2472853070
O	1.8541896973	-0.5905895603	-1.2472690339
O	0.9654127618	1.3590962348	-0.0000097477
N	-1.9568668142	-0.1910637806	-0.0000016260
O	-3.0682726487	-0.6280392756	0.0000018131
O	-1.8759710242	1.1847356751	-0.0000034230
O	-0.8998673608	-0.8125760556	-0.0000038702

H	-0.9133136759	1.3805084164	-0.0000066187

TS1

S	1.1509914276	-0.0157987988	0.0481684752
O	1.2119456976	-0.0834098655	1.4729888537
O	1.9531498697	-0.8159235831	-0.8097802405
O	0.7692264938	1.3272829841	-0.5033090535
N	-1.6358543302	-0.1469884680	-0.0452035365
O	-2.6691284068	-0.7194727887	0.0671484174
O	-1.5440312690	1.1300005649	0.0184320533
O	-0.5359934528	-0.8437310049	-0.2734267228
H	-0.4096150301	1.3941329601	-0.2387652464

P1

S	1.0171175782	-0.1025639362	0.1048191965
O	0.8587466919	0.3863385227	1.4368182128
O	1.9625887419	-1.0743525432	-0.3115154370
O	1.1155420506	1.1109649591	-0.9099228381
N	-1.6537489733	-0.0430082917	-0.0571775273
O	-2.6057219471	-0.7490726137	0.0176802671
O	-1.5297611413	1.1525747241	0.0194331409
O	-0.4318114498	-0.8127011253	-0.3455361257
H	0.5326484490	1.8200093042	-0.5797438893

Unscaled vibrational frequencies obtained at the DF-CCSD(T)-F12b/jun′-cc-pVDZ level

Frequencies (unit: cm^{-1}) :

HONO2
445.18 593.90 663.94 766.72 909.48
1353.57 1376.09 1799.03 3753.82

SO3
494.09 513.95 513.97 1049.12 1380.17 1380.20

C1
16.50 54.85 83.48 108.33 153.61 199.38 486.58 510.85
514.86 557.06 620.99 690.43 768.14 947.02 1052.29
1339.20 1368.94 1411.10 1431.82 1783.36 3603.09

TS1
901.80 i 86.75 102.14 263.83 325.00 375.82 470.29
520.33 530.63 669.81 752.10 787.67 806.58 1000.81
1064.14 1155.77 1272.20 1408.65 1454.00 1695.40
1796.14

P1

62.68 130.78 194.09 301.30 337.66 369.62 410.42
466.19 517.97 590.82 636.69 721.82 790.15 825.29
886.11 1194.99 1218.49 1351.11 1480.86 1816.06
3744.71

Rotational constants (unit: GHz):

HONO2
12.16952 6.28415 12.99411

SO3
5.11255 10.22509 10.22510

C1
0.96288 0.90639 3.82070

TS1
1.32462 1.22608 3.82891

P1
1.38612 1.26570 3.72815

Cartesian coordinates (Å) of the P1 product optimized by B3LYP/6-311+G(3df) method

P1

S	1.015679	-0.102026	0.105556
O	0.912734	0.394388	1.431380
O	1.952704	-1.073050	-0.309806
O	1.106003	1.094997	-0.914634
N	-1.682648	-0.040546	-0.055352
O	-2.615870	-0.761356	-0.041163
O	-1.574717	1.143546	0.050582
O	-0.420948	-0.807492	-0.299394
H	0.572665	1.839727	-0.592314

Unscaled vibrational frequencies of the P1 product obtained at the B3LYP/6-311+G(3df) level

P1
63.38 111.46 175.03 294.97 317.57 352.85 404.84
464.79 527.69 587.99 614.48 726.44 775.89 827.93
887.74 1183.10 1230.42 1345.54 1477.98 1789.76
3721.84

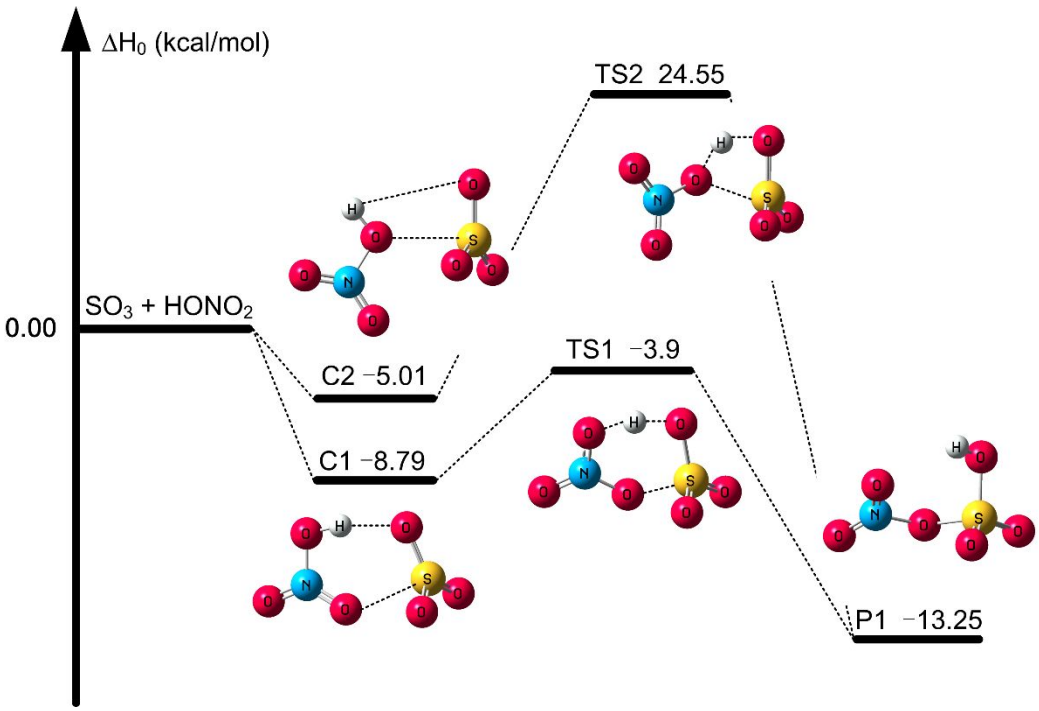

Figure S1. The calculated enthalpy profile at 0 K for the SO_3 + $HONO_2$ reaction at the M08-HX/MG3S level.

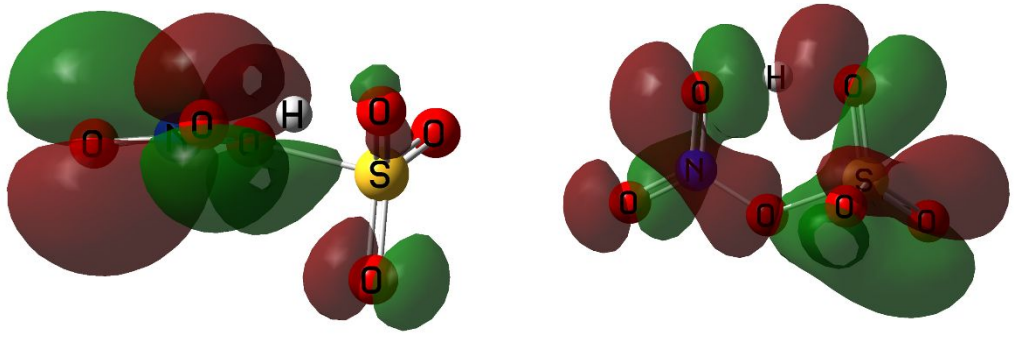

lp(O) $\sigma_{O\text{-}H}$

Figure S2. The natural orbitals for the lone pair of oxygen and the σ_{O-H} bonding of the transition state in the SO_3 + $HONO_2$ reaction.

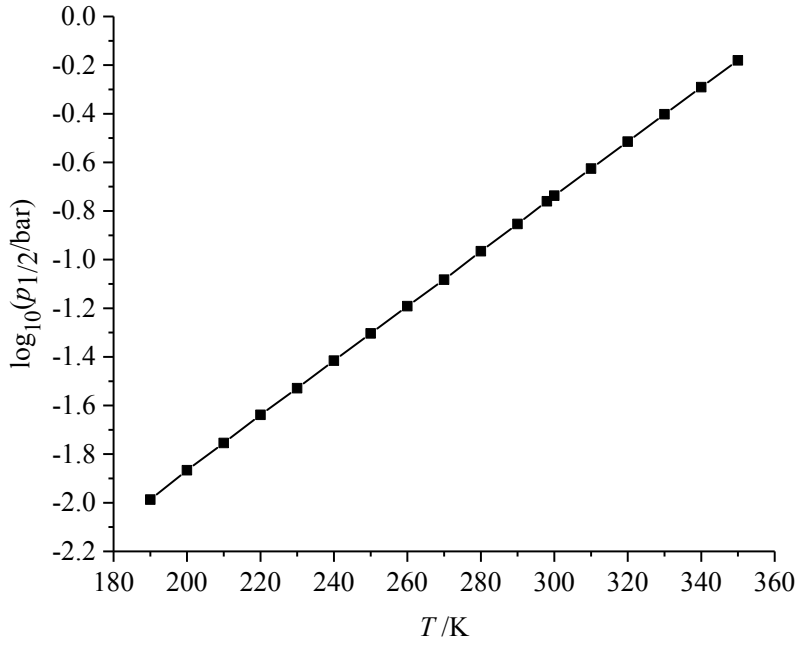

Figure S3. Transition pressure ($p_{1/2}$) of the SO_3 + $HONO_2$ reaction as a function of temperature for N_2 as bath gas.

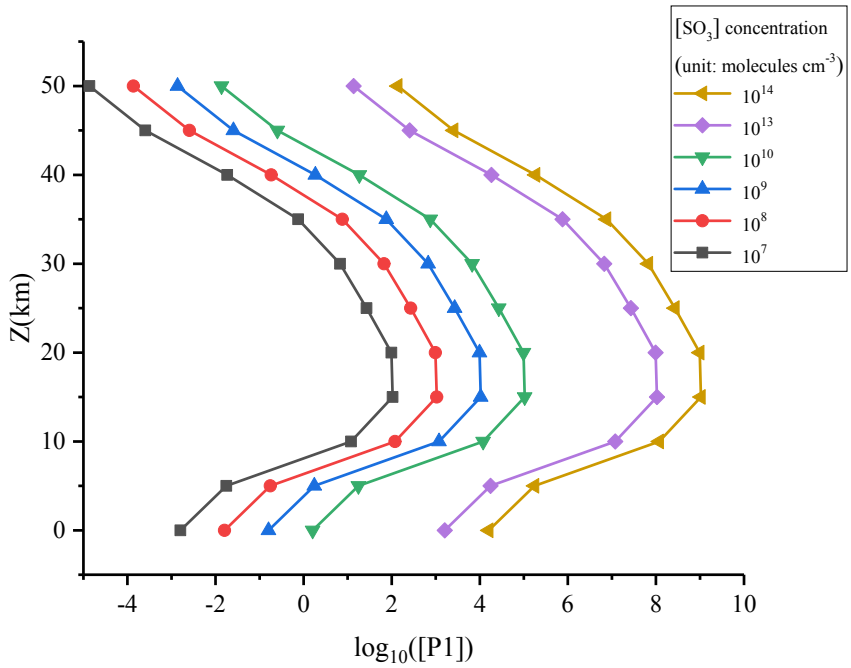

Figure S4. Concentration (unit: molecules cm^{-3}) of P1 with respect to different concentrations of SO_3 as function of altitude. We consider the possible concentrations of SO_3 with the injection of SO_3.

References

1 Chan, B.; Radom, L., W2X and W3X-L: Cost-Effective Approximations to W2 and W4 with kJ mol–1 Accuracy. *J. Chem. Theory Comput.* **2015**, *11*, 2109-2119.

2 Adler, T. B.; Knizia, G.; Werner, H.-J., A simple and efficient CCSD(T)-F12 approximation. *J. Phys. Chem.* **2007**, *127*, 221106.

3 Knizia, G.; Adler, T. B.; Werner, H.-J., Simplified CCSD(T)-F12 methods: Theory and benchmarks. *J. Phys. Chem*. **2009**, *130*, 054104.

4 Long, B.; Wang, Y.; Xia, Y.; He, X.; Bao, J. L.; Truhlar, D. G., Atmospheric Kinetics: Bimolecular Reactions of Carbonyl Oxide by a Triple-Level Strategy. *J. Am. Chem. Soc.* **2021**, *143*, 8402-8413.

5 Zhao, Y.; Truhlar, D. G., Exploring the Limit of Accuracy of the Global Hybrid Meta Density Functional for Main-Group Thermochemistry, Kinetics, and Noncovalent Interactions. *J. Chem. Theory Comput.* **2008**, *4*, 1849-1868.

6 Lynch, B. J.; Zhao, Y.; Truhlar, D. G., Effectiveness of Diffuse Basis Functions for Calculating Relative Energies by Density Functional Theory. *J. Phys. Chem. A* **2003***, 107,* 1384-1388.

7 Long, B.; Bao, J. L.; Truhlar, D. G., Atmospheric Chemistry of Criegee Intermediates: Unimolecular Reactions and Reactions with Water. *J. Am. Chem. Soc.* **2016***, 138,* 14409-14422.

8 Long, B.; Bao, J. L.; Truhlar, D. G., Kinetics of the Strongly Correlated CH3O + O2 Reaction: The Importance of Quadruple Excitations in Atmospheric and Combustion Chemistry. *J. Am. Chem. Soc.* **2019***, 141,* 611-617.

9 Bao, J. L.; Zheng, J.; Truhlar, D. G., Kinetics of Hydrogen Radical Reactions with Toluene Including Chemical Activation Theory Employing System-Specific Quantum RRK Theory Calibrated by Variational Transition State Theory. *J. Am. Chem. Soc.* **2016**, *138*, 2690-2704.

10 Bao, J. L.; Truhlar, D. G., Silane-initiated nucleation in chemically active plasmas: Validation of density functionals, mechanisms, and pressure-dependent variational transition state calculations. *Phys. Chem. Chem. Phys.* **2016**, *18*, 10097-10108.

11 Bao, J. L.; Truhlar, D. G., Variational transition state theory: theoretical framework and recent developments. *Chem. Soc. Rev.* **2017**, *46*, 7548-7596.

12 Troe, J., Predictive possibilities of unimolecular rate theory. *J. Phys. Chem.* **1979**, *83*, 114-126.

13 Bao, J. L.; Truhlar, D. G., Effect of energy dependence of the density of states on pressure-dependent rate constants. *Phys. Chem. Chem. Phys.* **2018**, *20*, 30475-30479.

14 R. G. Gilbert, K. L., and J. Troe., Theory of Thermal Unimolecular Reactions in the Fall-off Range. II. Weak Collision Rate Constants. *Phys. Chem.* **1983**, *87*, 169-177.

15 Kuwata, K. T. H., Matthew R., Carlson, Matthew J., Zogg, Cheryl K., Computational studies of the isomerization and hydration reactions of acetaldehyde oxide and methyl vinyl carbonyl oxide. *J. Phys. Chem. A* **2010**, *114*, 9192-204.

16 Tang, X.; Koenig, P. H.; Larson, R. G., Molecular Dynamics Simulations of Sodium Dodecyl Sulfate Micelles in Water—The Effect of the Force Field. *J. Phys. Chem. B* **2014**, *118*, 3864-3880.

17 J. O. Hirschfelder, C. F. Curtiss, and R. B. Bird, Molecular Theory of Gases and

Liquids, New York, Wiley, 1954.
18 (a) Lorentz, H. A., Ueber die Anwendung des Satzes vom Virial in der kinetischen Theorie der Gase. Ann. Phys. 1881, 248, 127-136. (b) Berthelot, D., "Sur le mélange des gaz", *Comptes. Rendus. Acad. Sci.* **1898**, *126*, 1703–1855
19 Alecu, I. M.; Zheng, J.; Zhao, Y.; Truhlar, D. G. Computational Thermochemistry: Scale Factor Databases and Scale Factors for Vibrational Frequencies Obtained from Electronic Model Chemistries. J. Chem. Theory Comput. 2010, 6, 2872-2887.
20 Georgievskii, Y.; Miller, J. A.; Burke, M. P.; Klippenstein, S. J. Reformulation and Solution of the Master Equation for Multiple-Well Chemical Reactions, J. Phys. Chem. A 2013, 117, 12146-12154.
21 Klippenstein, S. J. RRKM Theory and Its Implementation. Comprehensive Chem. Kinet. 2003, 39, 55-103.
22 Frisch, M. J.; Trucks, G. W.; Schlegel, H. B.; Scuseria, G. E.; Robb, M. A.; Cheeseman, J. R.; Scalmani, G.; Barone, V.; Petersson, G. A.; Nakatsuji, H.; Li, X.; Caricato, M.; Marenich, A. V; Bloino, J.; Janesko, B. G.; Gomperts, R.; Mennucci, B.; Hratchian, H. P.; Ortiz, J. V; Izmaylov, A. F.; Sonnenberg, J. L.; Williams-Young, D.; Ding, F.; Lipparini, F.; Egidi, F.; Goings, J.; Peng, B.; Petrone, A.; Henderson, T.; Ranasinghe, D.; Zakrzewski, V. G.; Gao, J.; Rega, N.; Zheng, G.; Liang, W.; Hada, M.; Ehara, M.; Toyota, K.; Fukuda, R.; Hasegawa, J.; Ishida, M.; Nakajima, T.; Honda, Y.; Kitao, O.; Nakai, H.; Vreven, T.; Throssell, K.; Montgomery Jr., J. A.; Peralta, J. E.; Ogliaro, F.; Bearpark, M. J.; Heyd, J. J.; Brothers, E. N.; Kudin, K. N.; Staroverov, V. N.; Keith, T. A.; Kobayashi, R.; Normand, J.; Raghavachari, K.; Rendell, A. P.; Burant, J. C.; Iyengar, S. S.; Tomasi, J.; Cossi, M.; Millam, J. M.; Klene, M.; Adamo, C.; Cammi, R.; Ochterski, J. W.; Martin, R. L.; Morokuma, K.; Farkas, O.; Foresman, J. B.; Fox, D. J. Gaussian 16, Revision A.03. 2016.
23 Frisch, M. J.; Trucks, G. W.; Schlegel, H. B.; Scuseria, G. E.; Robb, M. A.; Cheeseman, J. R.; Scalmani, G.; Barone, V.; Petersson, G. A.; Nakatsuji, H.; Li, X.; Caricato, M.; Marenich, A. V; Bloino, J.; Janesko, B. G.; Gomperts, R.; Mennucci, B.; Hratchian, H. P.; Ortiz, J. V; Izmaylov, A. F.; Sonnenberg, J. L.; Williams-Young, D.; Ding, F.; Lipparini, F.; Egidi, F.; Goings, J.; Peng, B.; Petrone, A.; Henderson, T.; Ranasinghe, D.; Zakrzewski, V. G.; Gao, J.; Rega, N.; Zheng, G.; Liang, W.; Hada, M.; Ehara, M.; Toyota, K.; Fukuda, R.; Hasegawa, J.; Ishida, M.; Nakajima, T.; Honda, Y.; Kitao, O.; Nakai, H.; Vreven, T.; Throssell, K.; Montgomery Jr., J. A.; Peralta, J. E.; Ogliaro, F.; Bearpark, M. J.; Heyd, J. J.; Brothers, E. N.; Kudin, K. N.; Staroverov, V. N.; Keith, T. A.; Kobayashi, R.; Normand, J.; Raghavachari, K.; Rendell, A. P.; Burant, J. C.; Iyengar, S. S.; Tomasi, J.; Cossi, M.; Millam, J. M.; Klene, M.; Adamo, C.; Cammi, R.; Ochterski, J. W.; Martin, R. L.; Morokuma, K.; Farkas, O.; Foresman, J. B.; Fox, D. J. Gaussian 16, Revision A.03. 2016.
24 Werner, H.-J.; Knowles, P. J.; Knizia, G.; Manby, F. R.; Schütz, M.; Celani, P.; Györffy, W.; Kats, D.; Korona, T.; Lindh, R.; Mitrushenkov, A.; Rauhut, G.; Shamasundar, K. R.; Adler, T. B.; Amos, R. D.; Bennie, S. J.; Bernhardsson, A.; Berning, A.; Cooper, D. L.; Deegan, M. J. O.; Dobbyn, A. J.; Eckert, F.; Goll, E.; Hampel, C.; Hesselmann, A.; Hetzer, G.; Hrenar, T.; Jansen, G.; Köppl, C.; Lee, S. J. R.; Liu, Y.; Lloyd, A. W.; Ma, Q.; Mata, R. A.; May, A. J.; McNicholas, S. J.; Meyer, W.; {Miller III}, T. F.; Mura, M. E.; Nicklaß, A.; O'Neill, D. P.; Palmieri, P.; Peng, D.; Pflüger, K.; Pitzer, R.; Reiher, M.; Shiozaki, T.; Stoll, H.; Stone, A.

J.; Tarroni, R.; Thorsteinsson, T.; Wang, M.; Welborn, M. *Molpro;* https://www.molpro.net (accessed June 6, 2021)

25 Zheng, J.; Bao, L. J. W.; Meana-Pañeda, R.; Zhang, S.; Lynch, B. J.; Corchado, J. C.; Chuang, Y.-Y.; Fast, P. L.; Hu, W.-P.; Liu, Y.-P.; Lynch, G. C.; Nguyen, K. A.;Jackels, C. F.; Fernandez-Ramos, A.; Ellingson, B. A.; Melissas, V. S.;Villa, J.; Rossi, I.; Coitino, L.; Pu, J.; Albu, T. V.; Steckler, R.; Garrett, B. C.; Issacson, A. D.; Truhlar, D. G. *Polyrate – version 2017-C*; University of Minnesota: Minneapolis, 2018.

26 Zheng, J.; Bao, L. J. W.; Zhang, S.; Corchado, J. C.; Chuang, Y.-Y.; Coitiño, E. L.; Ellingson, B. A.; Truhlar, D. G. *Gaussrate – version 2017-B;* University of Minnesota: Minneapolis, 2018.

27 Georgievskii, Y.; Klippenstein, S. J. MESS. http://tcg.cse.anl.gov/papr/codes/mess.html (accessed May 1, 2019).

28 Barbatti, M.; Aquino, A. J. A.; Lischka, H. The UV Absorption of Nucleobases: Semi-Classical Ab Initio Spectra Simulations. *Phys. Chem. Chem. Phys.* **2010**, *12*, 4959–4967.

29 Crespo-Otero, R.; Barbatti, M. Spectrum Simulation and Decomposition with Nuclear Ensemble: Formal Derivation and Application to Benzene, Furan and 2-Phenylfuran. *Theor. Chem. Acc.* **2012**, *131*, 1–14.

30 Sitkiewicz, S. P.; Rivero, D.; Oliva-Enrich, J. M.; Saiz-Lopez, A.; Roca-Sanjuán, D. Ab Initio Quantum-Chemical Computations of the Absorption Cross Sections of HgX2 and HgXY (X, y = Cl, Br, and I): Molecules of Interest in the Earth's Atmosphere. *Phys. Chem. Chem. Phys.* **2019**, *21*, 455–467.

31 Saiz-Lopez, A.; Sitkiewicz, S. P.; Roca-Sanjuán, D.; Oliva-Enrich, J. M.; Dávalos, J. Z.; Notario, R.; Jiskra, M.; Xu, Y.; Wang, F.; Thackray, C. P.; Sunderland, E. M.; Jacob, D. J.; Travnikov, O.; Cuevas, C. A.; Acuña, A. U.; Rivero, D.; Plane, J. M. C.; Kinnison, D. E.; Sonke, J. E. Photoreduction of Gaseous Oxidized Mercury Changes Global Atmospheric Mercury Speciation, Transport and Deposition. *Nat. Commun.* **2018**, *9*, 4796.

32 Saiz-Lopez, A.; Acuña, A. U.; Trabelsi, T.; Carmona-García, J.; Dávalos, J. Z.; Rivero, D.; Cuevas, C. A.; Kinnison, D. E.; Sitkiewicz, S. P.; Roca-Sanjuán, D.; Francisco, J. S. Gas-Phase Photolysis of Hg(I) Radical Species: A New Atmospheric Mercury Reduction Process. *J. Am. Chem. Soc.* **2019**, *141*, 8698–8702.

33 Francés-Monerris, A.; Carmona-García, J.; Acuña, A. U.; Dávalos, J. Z.; Cuevas, C. A.; Kinnison, D. E.; Francisco, J. S.; Saiz-Lopez, A.; Roca-Sanjuán, D. Photodissociation Mechanisms of Major Mercury(II) Species in the Atmospheric Chemical Cycle of Mercury. *Angew. Chemie - Int. Ed.* **2020**, *59*, 7605–7610.

34 Carmona-García, J.; Francés-Monerris, A.; Cuevas, C. A.; Trabelsi, T.; Saiz-Lopez, A.; Francisco, J. S.; Roca-Sanjuán, D. Photochemistry and Non-Adiabatic Photodynamics of the HOSO Radical. *J. Am. Chem. Soc.* **2021**, *143*, 10836–10841.

35 Carmona-García, J.; Trabelsi, T.; Francés-Monerris, A.; Cuevas, C. A.; Saiz-Lopez, A.; Roca-Sanjuán, D.; Francisco, J. S. Photochemistry of $HOSO_2$ and SO_3 and Implications for the Production of Sulfuric Acid. *J. Am. Chem. Soc.* **2021**, *143*, 18794–18802.

36 Wigner, E. On the Quantum Correction for Thermodynamic Equilibrium. *Phys. Rev.* **1932**, *40*, 749–759.

37 Barbatti, M.; Aquino, A. J. A.; Lischka, H., The UV absorption of nucleobases: semi-classical ab initio spectra simulations. *Phys. Chem. Chem. Phys.* **2010***, 12,* 4959-

4967.
38 Becke, A. D. Density-Functional Thermochemistry. III. The Role of Exact Exchange. *J. Chem. Phys.* **1993**, *98*, 5648–5652.
39 Lee, C.; Yang, W.; Parr, R. G. Development of the Colle-Salvetti Correlation-Energy Formula into a Functional of the Electron Density. *Phys. Rev. B* **1988**, *37*, 785–789.
40 McLean, A. D.; Chandler, G. S. Contracted Gaussian Basis Sets for Molecular Calculations. I. Second Row Atoms, Z=11-18. *J. Chem. Phys.* **1980**, *72*, 5639–5648.
41 Krishnan, R.; Binkley, J. S.; Seeger, R.; Pople, J. A. Self-Consistent Molecular Orbital Methods. XX. A Basis Set for Correlated Wave Functions. *J. Chem. Phys.* **1980**, *72*, 650–654.
42 Clark, T.; Chandrasekhar, J.; Spitznagel, G. W.; Schleyer, P. V. R. Efficient Diffuse Function-augmented Basis Sets for Anion Calculations. III. The 3-21+G Basis Set for First-row Elements, Li–F. *J. Comput. Chem.* **1983**, *4*, 294–301.
43 Barbatti, M.; Granucci, G.; Ruckenbauer, M.; Pittner, J. NEWTON-X: A Package for Newtonian Dynamics Close to the Crossing Seam. *Dynamics* **2007**, *16*, 3.
44 Barbatti, M.; Ruckenbauer, M.; Plasser, F.; Pittner, J.; Granucci, G.; Persico, M.; Lischka, H. Newton-X: A Surface-Hopping Program for Nonadiabatic Molecular Dynamics. *Wiley Interdiscip. Rev. Comput. Mol. Sci.* **2014**, *4*, 26–33.
45 Knowles, P. J.; Werner, H. J. An Efficient Second-Order MC SCF Method for Long Configuration Expansions. *Chem. Phys. Lett.* **1985**, *115*, 259–267.
46 Werner, H. J.; Knowles, P. J. A Second Order Multiconfiguration SCF Procedure with Optimum Convergence. *J. Chem. Phys.* **1985**, *82*, 5053–5063.
47 Roca-Sanjuán, D.; Aquilante, F.; Lindh, R. Multiconfiguration Second-Order Perturbation Theory Approach to Strong Electron Correlation in Chemistry and Photochemistry. *Wiley Interdiscip. Rev. Comput. Mol. Sci.* **2012**, *2*, 585–603.
48 Andersson, K.; Malmqvist, P. Å.; Roos, B. O. Second-Order Perturbation Theory with a Complete Active Space Self-Consistent Field Reference Function. *J. Chem. Phys.* **1992**, *96*, 1218–1226.
49 Roos, B. O.; Andersson, K.; Fülscher, M. P.; Malmqvist, P.-âke; Serrano-Andrés, L.; Pierloot, K.; Merchán, M. Multiconfigurational Perturbation Theory: Applications in Electronic Spectroscopy. **2007**, 219–331.
50 Andersson, K.; Malmqvist, P. Å.; Roos, B. O.; Sadlej, A. J.; Wolinski, K. Second-Order Perturbation Theory with a CASSCF Reference Function. *J. Phys. Chem.* **1990**, *94*, 5483–5488.
51 Finley, J.; Malmqvist, P. Å.; Roos, B. O.; Serrano-Andrés, L. The Multi-State CASPT2 Method. *Chem. Phys. Lett.* **1998**, *288*, 299–306.
52 Widmark, P.-O.; Persson, B. J.; Roos, B. O. Density Matrix Averaged Atomic Natural Orbital (ANO) Basis Sets for Correlated Molecular Wave Functions. *Theor. Chim. Acta* **1991**, *79*, 419–432.
53 Widmark, P.-O.; Malmqvist, P.-Å.; Roos, B. O. Density Matrix Averaged Atomic Natural Orbital (ANO) Basis Sets for Correlated Molecular Wave Functions. *Theor. Chim. Acta* **1990**, *77*, 291–306.
54 Fdez. Galván, I.; Vacher, M.; Alavi, A.; Angeli, C.; Aquilante, F.; Autschbach, J.; Bao, J. J.; Bokarev, S. I.; Bogdanov, N. A.; Carlson, R. K.; Chibotaru, L. F.; Creutzberg, J.; Dattani, N.; Delcey, M. G.; Dong, S. S.; Dreuw, A.; Freitag, L.; Frutos, L. M.; Gagliardi, L.; Gendron, F.; Giussani, A.; González, L.; Grell, G.; Guo, M.; Hoyer, C. E.; Johansson, M.; Keller, S.; Knecht, S.; Kovačević, G.; Källman, E.; Li Manni, G.; Lundberg, M.; Ma, Y.; Mai, S.; Malhado, J. P.; Malmqvist, P. Å.; Marquetand, P.; Mewes, S. A.; Norell, J.; Olivucci, M.; Oppel, M.; Phung, Q. M.;

Pierloot, K.; Plasser, F.; Reiher, M.; Sand, A. M.; Schapiro, I.; Sharma, P.; Stein, C. J.; Sørensen, L. K.; Truhlar, D. G.; Ugandi, M.; Ungur, L.; Valentini, A.; Vancoillie, S.; Veryazov, V.; Weser, O.; Wesołowski, T. A.; Widmark, P. O.; Wouters, S.; Zech, A.; Zobel, J. P.; Lindh, R. OpenMolcas: From Source Code to Insight. *J. Chem. Theory Comput.* **2019**, *15*, 5925–5964.

55 Aquilante, F.; Autschbach, J.; Baiardi, A.; Battaglia, S.; Borin, V. A.; Chibotaru, L. F.; Conti, I.; De Vico, L.; Delcey, M.; Galván, I. F.; Ferré, N.; Freitag, L.; Garavelli, M.; Gong, X.; Knecht, S.; Larsson, E. D.; Lindh, R.; Lundberg, M.; Malmqvist, P. Å.; Nenov, A.; Norell, J.; Odelius, M.; Olivucci, M.; Pedersen, T. B.; Pedraza-González, L.; Phung, Q. M.; Pierloot, K.; Reiher, M.; Schapiro, I.; Segarra-Martí, J.; Segatta, F.; Seijo, L.; Sen, S.; Sergentu, D. C.; Stein, C. J.; Ungur, L.; Vacher, M.; Valentini, A.; Veryazov, V. Modern Quantum Chemistry with [Open]Molcas. *J. Chem. Phys.* **2020**, *152*, 214117.

56 Ghigo, G.; Roos, B. O.; Malmqvist, P. Å. A Modified Definition of the Zeroth-Order Hamiltonian in Multiconfigurational Perturbation Theory (CASPT2). *Chem. Phys. Lett.* **2004**, *396*, 142–149.

57 Forsberg, N.; Malmqvist, P. Å. Multiconfiguration Perturbation Theory with Imaginary Level Shift. *Chem. Phys. Lett.* **1997**, *274*, 196–204.

58 Finlayson-Pitts, B. J.; Pitts Jr, J. N., *Chemistry of the upper and lower atmosphere: theory, experiments, and applications*. Elsevier: 1999. pp 61.

59 Madronich, S.; Flocke, S. The Role of Solar Radiation in Atmospheric Chemistry; 1999; pp 1–26.

60 Zheng, J.; Truhlar, D. G., Multi-path variational transition state theory for chemical reaction rates of complex polyatomic species: ethanol + OH reactions. *Faraday. Discuss.* **2012**, *157*, 59-88.

61 Bao, J. L.; Meana-Pañeda, R.; Truhlar, D. G., Multi-path variational transition state theory for chiral molecules: the site-dependent kinetics for abstraction of hydrogen from 2-butanol by hydroperoxyl radical, analysis of hydrogen bonding in the transition state, and dramatic temperature dependence of the activation energy. *Chem. Sci.* **2015**, *6*, 5866-5881.

62 Bao, J. L.; Zhang, X.; Truhlar, D. G., Predicting pressure-dependent unimolecular rate constants using variational transition state theory with multidimensional tunneling combined with system-specific quantum RRK theory: a definitive test for fluoroform dissociation. *Phys. Chem. Chem. Phys.* **2016**, *18*, 16659-16670.

63 Long, B.; Bao, J. L.; Truhlar, D. G. Reaction of SO_2 with OH in the Atmosphere. *Phys. Chem. Chem. Phys.* **2017**, *19*, 8091-8100.

64 Yao, L.; Fan, X.; Yan, C.; Kurtén, T.; Daellenbach, K. R.; Li, C.; Wang, Y.; Guo, Y.; Dada, L.; Rissanen, M. P.; Cai, J.; Tham, Y. J.; Zha, Q.; Zhang, S.; Du, W.; Yu, M.; Zheng, F.; Zhou, Y.; Kontkanen, J.; Chan, T.; Shen, J.; Kujansuu, J. T.; Kangasluoma, J.; Jiang, J.; Wang, L.; Worsnop, D. R.; Petäjä, T.; Kerminen, V.-M.; Liu, Y.; Chu, B.; He, H.; Kulmala, M.; Bianchi, F., Unprecedented Ambient Sulfur Trioxide (SO3) Detection: Possible Formation Mechanism and Atmospheric Implications. *Environ. Sci. Technol. Lett.* **2020,** *7*, 809-818.

65 Atkinson, R. *et al.* Evaluated kinetic and photochemical data for atmospheric chemistry: Volume I - gas phase reactions of Ox, HOx, NOx and SOx species. *Atmos. Chem. Phys.* **2004**, *4*, 1461-1738, doi:10.5194/acp-4-1461-2004.